Identification of Electrically Stressed Regions in AlGaN/GaN-on-Si Schottky Barrier Diode Using EBIC Technique

Juraj Priesol, Alexander Šatka, Aleš Chvála, Steve Stoffels, Brice De Jaeger, and Stefaan Decoutere

***Abstract*—The mapping of the current induced by a focused electron beam in a scanning electron microscope (SEM) has been used to localize electrically stressed regions in the AlGaN/GaN-on-Si Schottky barrier diode (SBD) structures cross-sectioned by the focused ion beam (FIB) technique. We have shown that homogeneously distributed electron beam induced current (EBIC) intensity detected below the Schottky contact at 0 V changes with increasing reverse voltage V_R and peaks at the edges of a field-plate region. The build-up of local microavalanches at high electric voltages has been indicated by overexposed EBIC signal at areas following the edges of the field plate structure. Interpretation of EBIC measurements is supported by electro-physical modeling and simulations employing the 2-D finite element method in Synopsys TCAD Sentaurus. The simulations prove that the electric field intensity in the SBD locally reaches values sufficiently high to trigger multiplication of the excessive carriers generated by an electron beam, which helps one to visualize and localize critical regions in GaN-based power electronic devices by the EBIC method.**

***Index Terms*—AlGaN/GaN, electric field, electrical stress, electron beam induced current (EBIC), focused ion beam (FIB), scanning electron microscopy, Schottky diode, TCAD simulation.**

Manuscript received September 10, 2020; revised October 23, 2020 and November 12, 2020; accepted November 15, 2020. This work has been supported by project PowerBase. This project has received funding from the Electronic Component Systems for European Leadership Joint Undertaking under grant agreement No. 662133. This Joint Undertaking receives support from the European Union's Horizon 2020 research and innovation programme and Austria, Belgium, Germany, Italy, Netherlands, Norway, Slovakia, Spain, and United Kingdom. Also, support from the the Slovak Research and Development Agency under Grant APVV-15-0673, and the Ministry of Education, Science, Research and Sport of the Slovak Republic through the Scientific Grant Agency under Grant 1/0746/19 is kindly acknowledged. The review of this article was arranged by Editor G. Meneghesso. *(Corresponding author: Juraj Priesol.)*

Juraj Priesol and Aleš Chvála are with the Institute of Electronics and Photonics, Slovak University of Technology in Bratislava, 81219 Bratislava, Slovakia (e-mail: juraj.priesol@stuba.sk; ales.chvala@stuba.sk).

Alexander Šatka is with the Institute of Electronics and Photonics, Slovak University of Technology in Bratislava, 812 19 Bratislava, Slovakia, and also with the IMS, Slovak Academy of Sciences, 841 04 Bratislava, Slovakia (e-mail: alexander.satka@stuba.sk).

Steve Stoffels, Brice De Jaeger, and Stefaan Decoutere are with the IMEC vzw, 3001 Leuven, Belgium (e-mail: brice.dejaeger@imec.be; stefaan.decoutere@imec.be).

Color versions of one or more figures in this article are available at https://doi.org/10.1109/TED.2020.3039756.

Digital Object Identifier 10.1109/TED.2020.3039756

I. Introduction

THE unceasing progress in the development of GaN heterojunction devices calls for a rapid development of measurement methods and procedures, which provide new and valuable information about their electrical and physical properties. The unique nature of GaN altogether with high-power switching capabilities of GaN hetero-junction devices makes these structures attractive for power electronics with a remarkable impact on many areas of everyday life and industry [1]–[3]. Alongside a range of standard methods used for thorough characterization, special techniques are constantly developed to understand the electrical behavior of GaN devices under different bias conditions. Especially interesting are methods allowing the identification of regions with excessive electrical and/or optical activity. Only recently, the surface potential of cross-sectioned AlGaN/GaN high electron mobility transistor (HEMT) has been successfully visualized by Kelvin probe force microscopy (KPFM) [4]. Melitz *et al.* [5] pointed out the importance of perfectly smooth surface at the cross section due to a significant influence of abrupt topographic height on the KPFM signal and its interpretation. Required smoothness has been achieved by a special triple ion beam cutting technique eliminating the effect of disparate mill-rates of the materials in the HEMT structure. Alternative methods to the KPFM, which are slightly less affected by the quality of prepared cross sections, are based on the measurement of currents induced in the sample by a beam of accelerated electrons (EBIC - electorn beam induced current) [6] or ions (IBIC - ion beam induced current) [7]. Since the excessive carriers are generated in the sample volume under the surface, EBIC and IBIC signals are less sensitive to the surface imperfection while the spatial resolution is in the order of tens of nm; this depends essentially on the e-beam energy, material parameters as well as the complexity of the investigated structure. Obviously, such resolutions cannot outperform the ones provided by the KPFM but are acceptable when large-scale power electronic devices are being investigated. From the application point of view, IBIC is more suitable for the investigation of buried structures thanks to the long-range and low lateral scattering of MeV ions [7]. Therefore, nondestructive analysis is possible only if small ion doses are sufficient to obtain good-quality images [8]. Since the energy of accelerated electrons in nowadays scanning electron microscopes (SEMs) is approximately three orders of magnitude lower (typically between 1 and 20 keV), the problem with the beam-induced damage is not as significant as in the IBIC method. It is worth mentioning that comparable nondestructive analyses can also be performed by the measurement of currents induced in semiconductors by a fine-focused light beam, e.g., by light or laser beam induced current (LBIC) and optical beam induced current (OBIC) methods [9]. The advantage of these techniques is they can be performed at open air conditions; however, they provide relatively low spatial resolution in the order of hundreds of nanometers at best (except a high-injection level conditions or special structures with the resolution limited by the size of the nanoobjects).

Following from this short overview, the EBIC method is a reasonable option for the investigation of electrically stressed regions in GaN-based heterostructure devices. Moreover, it can also be used for the visualization and localization of defects, which are electrically active at various voltages and could contribute to the leakage currents in GaN buffer stacks [10]–[12]. Another utilization of the EBIC method includes the investigation of local electronic transport properties of devices at a high spatial resolution [13]–[15], direct visualization of p-n and Schottky junctions in planar [16] and advanced 3-D structures [17]–[19] as well as the investigation of doping mechanisms of semiconductor structures at the nanoscale [20].

The aim of this work is the adaptation and further advancement of the EBIC method for the assessment of the electric field distribution at the cross section of AlGaN/GaN-on-Si Schottky barrier diode (SBD) during *in situ* biasing. The main goal is to identify regions of critical electric field intensities in the structure, which is a fundamental step toward the development of more reliable and robust power electronic devices and circuits.

II. Experimental

The AlGaN/GaN-on-Si SBDs were fabricated by metal–organic chemical vapor deposition (MOCVD) on GaN-on-Si wafers. The vertical structure and technology used for the preparation of a conventional SBD is described in detail in [21]. Here, it is worth to mention that the epitaxial structure is comprised of 17-nm thick $Al_{0.21}Ga_{0.79}N$ barrier, 150-nm thick unintentionally doped GaN channel, and 2600-nm thick $Al_xGa_{1-x}N$ buffer stack grown on 200-nm thick AlN nucleation layer on p-type Si (111) substrate. The cathode contact is formed by Au-free Ti/Al/Ti/TiN-based stack, whilst the anode contact consists of 20 nm TiN/20 nm Ti/250 nm Al/20 nm Ti/60 nm TiN stack.

Initially, simple mechanical cleaving was used to prepare a vertical cross section of SBD devices. This approach has been found unreliable due to a metal burr and remnants on the cross-sectioned surface influencing the EBIC signal, mostly in the region of high electric fields; mechanical sliding of the burrs or remnants by nanoprobe does not help to solve the problem. Therefore, an alternative approach using focused ion beam (FIB) etching has been used for selective physical milling and preparation of precise and clean cross sections.

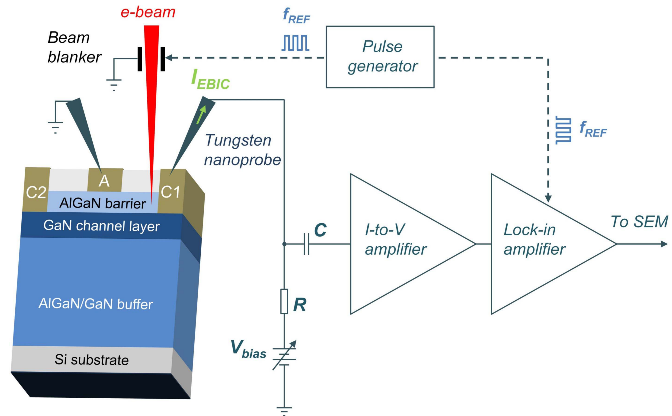

Fig. 1. EBIC setup with investigated AlGaN/GaN-on-Si Schottky barrier diode cross-section.

It has been assumed that the surface layer influenced by ion milling is very thin in comparison to the EBIC generation volume.

Room temperature EBIC experiments were performed using field emission gun (FEG) SEM LEO-1550 at e-beam energies $E_{pe} = 3$ and 5 keV and beam current $I_{pe} \leq 100$ pA. Investigated SBD structure was contacted by tungsten probes positioned by micromanipulators Kleindiek MM3A-EM equipped with the low-resistance and low-noise probe tip holders LCMK-EM. Glass isolation was inserted between the sample and sample holder to avoid possible leakage paths through the substrate. EBIC was measured laterally between the anode and one of the cathode electrodes at reverse bias, as is illustrated in Fig. 1. During the experiment, the e-beam is scanning over the selected area at the surface of the SBD cross section. Incident electrons penetrate below the surface and dissipate their energy via inelastic scattering collisions with the sample atoms. This process is accompanied by the generation of various signals (e.g., secondary electrons (SEs), characteristic X-rays, Auger electrons) including the generation of excessive electron–hole pairs, which are separated by internal electric fields. As a result, drift/diffusion of these excessive carriers reaching neutral regions can be measured as EBIC signal I_{EBIC}.

To measure and map the spatial distribution of induced currents in the order of 10^{-6} A and below, the generated EBIC signal has been preamplified and subsequently adjusted using transimpedance amplifier to fit the voltage input of the lock-in amplifier. Beam-blanking technique with phase-synchronous detection has been used to allow for the measurement of low-intensity EBIC signals. The interpretation of EBIC measurements has been supported by TCAD modeling [22] of examined structures using the finite element method to simulate the electric field distribution in the SBD structure.

III. Results and Discussion

SEM-SE top-view and bird's eye view micrographs of the investigated planar AlGaN/GaN-on-Si SBD structure with vertical cross section prepared by FIB milling are shown in Fig. 2. The FIB cross section of the back-to-back diode structures

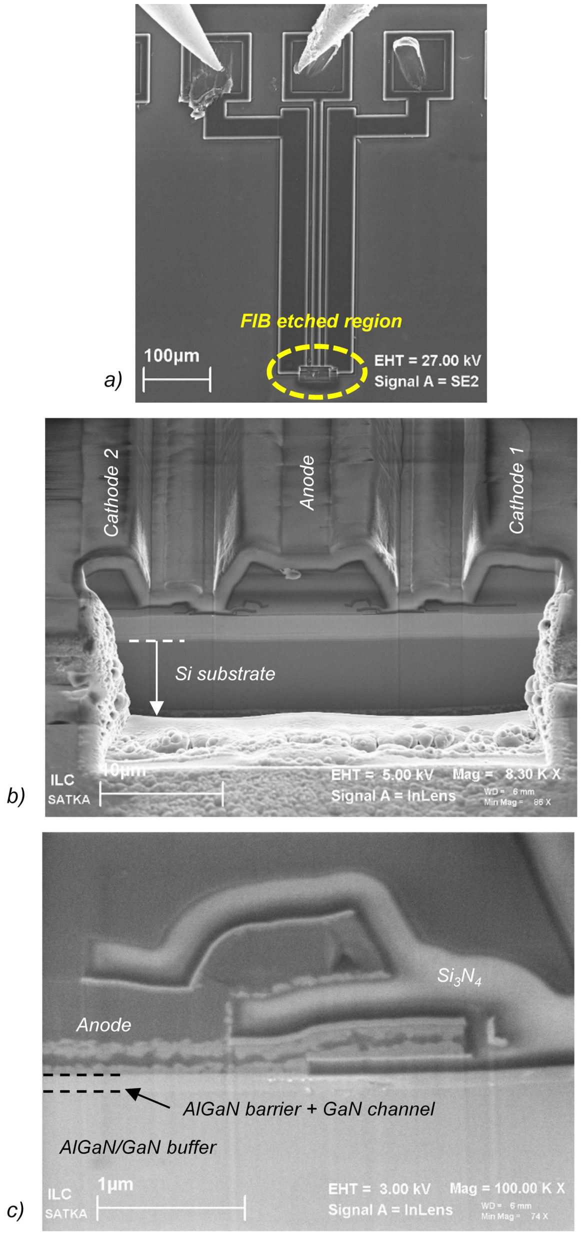

Fig. 2. (a) SEM-SE top-view image of AlGaN/GaN-on-Si SBD with encircled FIB cross section. (b) Bird's eye view of the cross-sectioned region. (c) Field-plate structure at the anode edge from the cathode 1 side.

has been prepared at the very end of the electrode fingers [Fig. 2(a)] where the anode metal contact is situated between two cathode contacts marked in Fig. 2(b) as "Cathode 1" and "Cathode 2." The ~35-μm wide FIB crater is large enough to inspect the whole anode area and possibly an active part of the cathodes. The detail of the anode rim from the "Cathode 1" side in Fig. 2(c) shows the anode metal formed to field-plate structure altogether with ~170-nm thick AlGaN/GaN heterostructure prepared on the $Al_xGa_{1-x}N$ buffer stack; note that the graphical scales in Fig. 2(b) and (c) are valid in the horizontal direction only, due to a ~45° orientation of the sample relative to the incident e-beam.

During the EBIC measurements, only one cathode came into contact with a tungsten probe tip while the other one

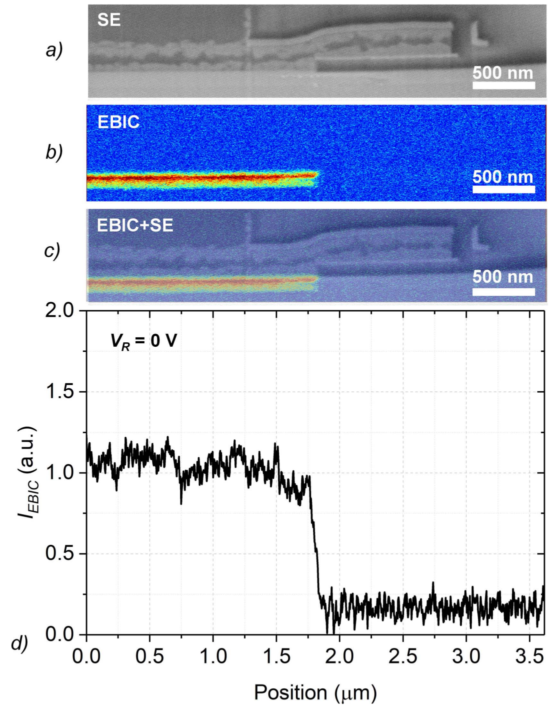

Fig. 3. (a) SEM-SE micrograph, (b) colored EBIC map, and (c) overlaid SEM-SE micrograph and EBIC map of the anode edge region at 0 V acquired at e-beam energy $E_{pe} = 3$ keV. (d) Also shown is the corresponding EBIC profile obtained by the integration of EBIC intensity map in vertical direction. Images (a)–(c) are scaled equally to the *x*-axis in (d).

remained floating. In this configuration, the EBIC signal at $V_R = 0$ V between the anode and one of the cathodes has been detected from the whole region under the Schottky contact due to high electron mobility in the two-dimensional electron gas (2DEG) formed in GaN at the AlGaN/GaN heterointerface. The spatial distribution of EBIC intensity close to the anode edge from the "Cathode 1" side can be deduced from the comparison of SEM-SE micrograph in Fig. 3(a) and corresponding EBIC map in Fig. 3(b), which are overlaid in Fig. 3(c). The amplitude of the EBIC maximum at 0 V is practically constant under the Schottky contact indicating good spatial homogeneity of the built-in electric field adjacent to the anode-metal/semiconductor interface. Nevertheless, a careful inspection reveals slightly lower EBIC signal intensity at the anode rim close to the field plate, in accordance with expectations. This trend is apparent also from the EBIC line profile in Fig. 3(d) extracted from the EBIC map in Fig. 3(b) by numerical integration in the vertical direction.

With increasing reverse voltage, the amplitude of the EBIC signal under the anode metal contact remained practically independent of the reverse voltage V_R. In contrast, the EBIC signal at the edge of the anode metal started to locally increase with the V_R so that at $V_R = 60$ V it has increased more than two orders of magnitude relative to 0-V EBIC value at the anode metal edge. This redistribution of the EBIC signal is obvious from the comparison of SEM-SE images of the same region in Fig. 4(a) and EBIC map in Fig. 4(b), which are overlaid in Fig. 4(c).

Low dependence of the EBIC amplitude on reverse voltage under the Schottky contact results from the facts that:

This article has been accepted for inclusion in a future issue of this journal. Content is final as presented, with the exception of pagination.

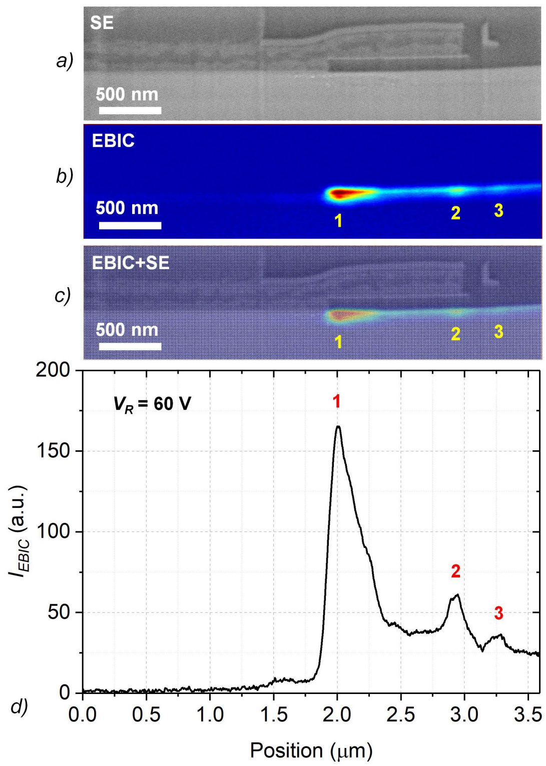

Fig. 4. (a) SEM-SE micrograph, (b) colored EBIC map, and (c) overlaid SEM-SE micrograph and EBIC map of the anode edge region at reverse voltage of $V_R = 60$ V acquired at e-beam energy $E_{pe} = 3$ keV. (d) Also shown is the corresponding EBIC profile obtained by the integration of EBIC intensity map in vertical direction. Images (a)–(c) are scaled equally to the x-axis in (d). EBIC signal intensity is approximately two orders of magnitude higher than that measured at 0 V in Fig. 3.

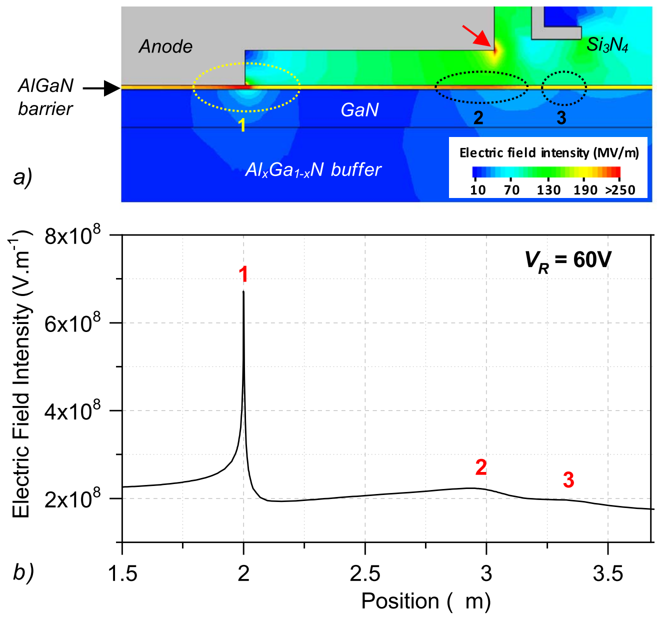

Fig. 5. (a) TCAD simulation of the electric field intensity distribution in the SBD structure at the rim of the Schottky metal contact at reverse voltage of $V_R = 60$ V. (b) Simulated electric field intensity line distribution inside AlGaN barrier layer in the depth of ~0.5 nm from the Schottky metal contact.

1) electric field intensity increases mostly in the AlGaN layer at the Schottky contact/AlGaN layer heterointerface; 2) holes (electrons) generated by e-beam are effectively collected by Schottky contact (2DEG) already at 0 V so that the number of carriers collected by space charge region (SCR) with increasing reverse voltage is nearly constant; 3) widening of the SCR under the anode metal is strongly modified by 2DEG at the potential of the "Cathode 1;" and 4) the number of excessive carriers generated by e-beam remains constant up to some critical electric field intensity. This effect can be compared to a nearly constant generation of the photocurrent in p-i-n photodiodes at reverse voltages below avalanche breakdown conditions. In contrast, a significant increase of the EBIC signal at the perimeter of the anode contact directly indicates the redistribution of the electric field with reverse voltage resulting in local avalanche multiplication of the generated carriers at the edge of the Schottky contact metal under the field plate. At these conditions, carriers generated by e-beam are accelerated in a locally increased electric field and are multiplied by impact ionization, which results in a dramatic increase of EBIC signal intensity in region "1" indicated in Fig. 4(b) and (c). Moreover, a closer look at the EBIC map in Fig. 4(b) reveals additional EBIC maxima spatially assigned to regions "2" and "3" of the GaN channel layer, which is well perceptible from the extracted EBIC profile in Fig. 4(d).

The EBIC amplitude in regions 2 and 3 is remarkably lower than that in region 1, indicating comparably lower electric fields and so lower carrier multiplication of generated carriers due to an exponential dependence of the avalanche ionization coefficients of generated carriers on the electric field intensity [23], [24]. It is worth mentioning that although all three regions are located at the rim of the Schottky metal contact, the visualization of their electrical activity is possible thanks to a high lateral conductivity at the AlGaN/GaN heterointerface, where extraction of the carriers takes place through the 2DEG in the GaN channel.

To support these observations, a 2-D model of the structure with the same field-plate geometry was designed and used for electro-physical simulations and further analysis in TCAD. Polarization charges at the interfaces are computed by a strain piezoelectric polarization model [25] and the electrical simulation is performed by the drift-diffusion model. Simulated distribution of electric field at a bias voltage of $V_R = 60$ V in Fig. 5 shows four high-intensity regions, three of which are encircled by dashed lines and labeled as 1, 2, and 3, and the fourth one is indicated by the red arrow. Region 1 is located at the edge of the anode metal contact, which is consistent with the EBIC measurement presented in Fig. 4(b). Simulated electric field intensity in this area reaches about 6.5×10^8 V/m, which is sufficient to trigger local microavalanche multiplication of the excessive carriers generated by the electron beam (critical electric field intensity for the onset of the avalanche breakdown in GaN reaches $\sim 1.5 \times 10^8$ Vm^{-1}, ionization coefficients for electrons and holes exceed the value of 10^7 m^{-1} at electric field intensity above 5×10^8 Vm^{-1} [23], [24]). The electrical stress of such intensity locally concentrated to a relatively small volume leads to a gradual hot-carrier degradation of the device negatively influencing its long-term stability and lifetime (see e.g., [26], [27] and references therein). The kinetic energy of the hot carriers undergoing the avalanching is finally transformed to local overheating of a small device volume and leads to a gradual degradation of the device. In addition, such conditions may result in a sudden unrecoverable thermal degradation of the device at the Schottky gate edge.

One of the most promising topologies to reduce the electric field in region 1 involves embedding a thin Si_3N_4 layer as the edge termination inside the anode trench, which has been reported in [28] as Gated Edge Terminated SBD architecture. In addition to region 1, channel region 2 with EBIC maximum located under the field plate edge as well as region 3 was also found to be under higher electrical stress, which is in good agreement with increased EBIC intensity in these areas. It is worth mentioning that the contribution of the investigated avalanching localized at the rim of the Schottky anode to the total reverse leakage is nearly inversely proportional to the Schottky contact area making it difficult to distinguish in $I-V$ curves of large area power SBD diodes.

Nevertheless, further correlation of EBIC measurements and TCAD simulations shows a difference in the insulator region indicated in Fig. 5 by the red arrow revealing a relatively high intensity of the electric field at the edge of the field-plate. On the contrary, no EBIC signal has been detected from this area [cf., in Fig. 4(b) and (c)] indicating good dielectric strength of the insulating layer. Identification of this region from simulations is important, since the further increase of reverse bias in similar structures may lead to a significant increase of the electric field in this area resulting in a fatal failure of the device due to an irreversible dielectric breakdown. Such an increase of electric field in the insulating layer is also consistent with the results reported in [29], where high electric field intensity has been confirmed by simulations at the gate-head edge of a GaN HEMT in OFF-state under a high drain bias.

IV. Conclusion

Regions of a critical electric field in planar AlGaN/GaN-on-Si SBD heterostructures have been experimentally localized by mapping of the current induced by a focused electron beam in electrically biased samples with cross section prepared by FIB technique. EBIC mapping of the SBD structures revealed that homogeneously distributed EBIC intensity below the Schottky anode at 0 V is significantly redistributed with increasing reverse voltage (to $V_R = 60$ V in this particular structure) and the electric field increases to critical values under the edges of the field plate structure. TCAD electro-physical simulations of the structure proved that the electric field intensity at $V_R = 60$ V between the anode and the cathode can be locally sufficiently high to trigger the multiplication of carriers by a local microavalanche breakdown, which has been identified from the local increase of the EBIC intensity. The spatial analysis confirmed a good correlation between the high electric field regions predicted by electro-physical simulations and high-intensity regions observed in EBIC maps. Moreover, TCAD simulations with the model structure adjusted according to EBIC observations helped to identify an additional electrically stressed region in the Si_3N_4 layer adjacent to the edge of the field plate structure. Localization of these regions, whether predicted theoretically or confirmed experimentally, is essential for further optimization of these structures leading to the development of more reliable and robust GaN power electronic devices.

References

[1] S. J. Pearton, F. Ren, A. P. Zhang, and K. P. Lee, "Fabrication and performance of GaN electronic devices," *Mater. Sci. Eng., R, Rep.*, vol. 30, nos. 3–6, pp. 55–212, Dec. 2000, doi: 10.1016/S0927-796X(00)00028-0.

[2] O. Ambacher *et al.*, "Two-dimensional electron gases induced by spontaneous and piezoelectric polarization charges in N-and Ga-face AlGaN/GaN heterostructures," *J. Appl. Phys.*, vol. 85, no. 6, pp. 3222–3233, Mar. 1999, doi: 10.1063/1.369664.

[3] U. K. Mishra, S. Likun, T. E. Kazior, and Y.-F. Wu, "GaN-based RF power devices and amplifiers," *Proc. IEEE*, vol. 96, no. 2, pp. 287–305, Feb. 2008, doi: 10.1109/JPROC.2007.911060.

[4] A. M. Hilton, J. L. Brown, E. A. Moore, J. A. Hoelscher, E. R. Heller, and D. L. Dorsey, "Characterization of cross-sectioned gallium nitride high-electron-mobility transistors with *in situ* biasing," *J. Electron. Mater.*, vol. 44, no. 10, pp. 3259–3264, Jul. 2015, doi: 10.1007/s11664-015-3908-0.

[5] W. Melitz, J. Shen, A. C. Kummel, and S. Lee, "Kelvin probe force microscopy and its application," *Surf. Sci. Rep.*, vol. 66, no. 1, pp. 1–27, Jan. 2011, doi: 10.1016/j.surfrep.2010.10.001.

[6] H. J. Leamy, "Charge collection scanning electron microscopy," *J. Appl. Phys.*, vol. 53, no. 6, pp. R51–R80, Jun. 1982, doi: 10.1063/1.331667.

[7] M. B. H. Breese, E. Vittone, G. Vizkelethy, and P. J. Sellin, "A review of ion beam induced charge microscopy," *Nucl. Instrum. Methods Phys. Res. B, Beam Interact. Mater. At.*, vol. 264, no. 2, pp. 345–360, Nov. 2007, doi: 10.1016/j.nimb.2007.09.031.

[8] T. Osipowicz *et al.*, "IBIC analysis of high-power devices," *Nucl. Instrum. Methods Phys. Res. B, Beam Interact. Mater. At.*, vol. 181, nos. 1–4, pp. 311–314, Jul. 2001, doi: 10.1016/S0168-583X(01)00487-6.

[9] J. Domaradzki and D. Kaczmarek, "Optical beam injection methods as a tool for analysis of semiconductor structures," *Optica Applicata*, vol. 35, no. 1, pp. 129–137, 2005.

[10] H. Lu *et al.*, "Schottky rectifiers fabricated on bulk GaN substrate analyzed by electron-beam induced current technique," *Solid-State Electron.*, vol. 52, no. 5, pp. 817–823, May 2008, doi: 10.1016/j.sse.2007.10.053.

[11] J. Kováč, A. Šatka, A. Chvála, D. Donoval, P. Kordoš, and S. Delage, "Gate leakage current in GaN-based mesa- and planar-type heterostructure field-effect transistors," *Microelectron. Rel.*, vol. 52, no. 7, pp. 1323–1327, Jul. 2012, doi: 10.1016/j.microrel.2012.02.003.

[12] H. Umezawa *et al.*, "Defect and field-enhancement characterization through electron-beam-induced current analysis," *Appl. Phys. Lett.*, vol. 110, no. 18, May 2017, Art. no. 182103, doi: 10.1063/1.4982590.

[13] O. Marcelot, S. I. Maximenko, and P. Magnan, "Plan view and cross-sectional view EBIC measurements: Effect of e-beam injection conditions on extracted minority carrier transport properties," *IEEE Trans. Electron Devices*, vol. 61, no. 7, pp. 2437–2442, Jul. 2014, doi: 10.1109/TED.2014.2323997.

[14] S. I. Maximenko *et al.*, "Radiation response of multi-quantum well solar cells: Electron-beam-induced current analysis," *J. Appl. Phys.*, vol. 118, no. 24, Dec. 2015, Art. no. 245705, doi: 10.1063/1.4939067.

[15] E. B. Yakimov, "What is the real value of diffusion length in GaN?" *J. Alloys Compounds*, vol. 627, pp. 344–351, Apr. 2015, doi: 10.1016/j.jallcom.2014.11.229.

[16] S. I. Maximenko, S. R. Messenger, C. D. Cress, J. A. Freitas, and R. J. Walters, "Application of CL/EBIC-SEM techniques for characterization of radiation effects in multijunction solar cells," *IEEE Trans. Nucl. Sci.*, pp. 3095–3100, Dec. 2010, doi: 10.1109/TNS.2010.2083691.

[17] M. Tchernycheva *et al.*, "Core–shell InGaN/GaN nanowire light emitting diodes analyzed by electron beam induced current microscopy and cathodoluminescence mapping," *Nanoscale*, vol. 7, no. 27, pp. 11692–11701, Jun. 2015, doi: 10.1039/c5nr00623f.

[18] P. Tchoulfian, F. Donatini, F. Levy, A. Dussaigne, P. Ferret, and J. Pernot, "Direct imaging of p–n junction in core–shell GaN wires," *Nano Lett.*, vol. 14, no. 6, pp. 3491–3498, May 2014, doi: 10.1021/nl5010493.

[19] I. Gîrgel *et al.*, "Optical characterization of magnesium incorporation in p-GaN layers for core–shell nanorod light-emitting diodes," *J. Phys. D, Appl. Phys.*, vol. 51, no. 15, p. 155103, Mar. 2018, doi: 10.1088/1361-6463/aab16b.

[20] J. D. Poplawsky, C. Li, N. R. Paudel, W. Guo, Y. Yan, and S. J. Pennycook, "Nanoscale doping profiles within CdTe grain boundaries and at the CdS/CdTe interface revealed by atom probe tomography and STEM EBIC," *Sol. Energy Mater. Sol. Cells*, vol. 150, pp. 95–101, Jun. 2016, doi: 10.1016/j.solmat.2016.02.004.

[21] J. Hu, S. Lenci, S. Stoffels, B. D. Jaeger, G. Groeseneken, and S. Decoutere, "Leakage-current reduction and improved on-state performance of au-free AlGaN/GaN-on-Si Schottky diode by embedding the edge terminations in the anode region," *Phys. Status Solidi (C)*, vol. 11, nos. 3–4, pp. 862–865, Feb. 2014, doi: 10.1002/pssc.201300472.

[22] *Sentaurus Device User Guide, Version N-2017.09*, Synopsys TCAD Sentaurus, San Jose, CA, USA, 2017.

[23] I. H. Oğuzman, E. Bellotti, K. F. Brennan, J. Kolník, R. Wang, and P. P. Ruden, "Theory of hole initiated impact ionization in bulk zincblende and wurtzite GaN," *J. Appl. Phys.*, vol. 81, no. 12, pp. 7827–7834, Jun. 1997, doi: 10.1063/1.365392.

[24] L. Cao *et al.*, "Experimental characterization of impact ionization coefficients for electrons and holes in GaN grown on bulk GaN substrates," *Appl. Phys. Lett.*, vol. 112, no. 26, Jun. 2018, Art. no. 262103, doi: 10.1063/1.5031785.

[25] *Simulation of Silicon Substrate Effect on AlGaN/GaN HFET Off-State Breakdown Voltage*, Synopsys, Mountain View, CA, USA, 2016.

[26] Ch. Hu, S. C. Tam, F-Ch. Hsu, P-K. Ko, T.-Y. Chan, k, W. Terrill, "Hot-electron-induced MOSFET degradation-model, monitor, and improvement," *IEEE Trans. Electronic Devices*, vol. 32, no. 2, pp. 375–385, Apr. 1985.

[27] G. Meneghesso *et al.*, "Degradation of AlGaN/GaN HEMT devices: Role of reverse-bias and hot electron stress," *Microelectron. Eng.*, vol. 109, pp. 257–261, Sep. 2013, doi: 10.1016/j.mee.2013.03.017.

[28] S. Lenci *et al.*, "Au-free AlGaN/GaN power diode on 8-in Si substrate with gated edge termination," *IEEE Electron Device Lett.*, vol. 34, no. 8, pp. 1035–1037, Aug. 2013, doi: 10.1109/LED.2013.2267933.

[29] M. Meneghini, O. Hilt, J. Wuerfl, and G. Meneghesso, "Technology and reliability of normally-off GaN HEMTs with p-Type gate," *Energies*, vol. 10, no. 2, p. 153, Jan. 2017, doi: 10.3390/en10020153.